How random is dice tossing?

Jan Nagler[1,2] and Peter Richter[2]
[1]*Max Planck Institute for Dynamics and Self-Organization, Göttingen, Germany*
and Institute for Nonlinear Dynamics, Georg August University Göttingen, Bunsenstraße 10, D-37073 Göttingen, Germany
[2]*Institute for Theoretical Physics, University of Bremen, Otto-Hahn-Allee, D-28334 Bremen, Germany*
(Received 27 June 2008; published 8 September 2008)

Tossing the dice is commonly considered a paradigm for chance. But where in the process of throwing a cube does the randomness reside? After all, for all practical purposes the motion is described by the laws of deterministic classical mechanics. Therefore the undisputed status of dice as random number generators calls for a careful analysis. This paper is an attempt in that direction. As a simplified model of a dice a barbell with two marked masses at its tips and only two final positions is considered. It is shown how, depending on initial conditions and the degree of dissipation during bounces, the outcome is only more or less unpredictable: the system is not truly random but pseudorandom—even under conditions where it appears to be random.

DOI: 10.1103/PhysRevE.78.036207 PACS number(s): 05.45.Ac, 45.05.+x

I. INTRODUCTION

Dice throwing is perceived as epitomizing randomness. Everybody is familiar, from childhood on, with cubic dice as part of board games such as backgammon. Sometimes, such as in role-playing games, other dice geometries are used, ranging from 7-sided, over 34-sided, to even 100-sided dice [1], but all of them are assumed to be perfect random number generators. When Einstein wrote in a letter to Born (1926) "I, at any rate, am convinced that *He* does not play dice" [2], thereby objecting to the view that the basic laws of nature incorporate randomness, he took it for granted that dice tossing is a random process. Starting in the mid-seventies, the theory of dynamical systems introduced the notion of *deterministic chaos* to refer to the observation that randomness may be generated on the basis of purely classical mechanics. Hence it became conceivable that dice throwing may at the same time be described by perfectly deterministic laws, and yet produce sequences of random numbers.

However, the implementation of this idea in terms of explicit calculations has never been carried out. In the literature only a few scientifically motivated experiments to test fair dice and coins have been reported, see [3] for a recent review. Theoretical work has mainly focused on simulations of simple models with two-sided or four-sided dice. Vulović and Prange studied the basins of attraction of the two possible final configurations of a homogeneous rod [4]; Feldberg *et al.* focused on a rolling square and the corresponding final states for varying initial conditions [5]; Ford and Kechen studied throws of a homogeneous disk [6,7], and the edge landing of a coin was modeled by Murray and Teare [8].

General experience with chaotic dynamical systems as well as simple home experiments support the expectation that the degree of randomness in dice throwing depends on the circumstances, notably on initial conditions. Rarely is motion completely chaotic: from the point of view of phase space geometry, regions of regular motion are more or less intimately mixed with regions of chaos; from the dynamical point of view, chaos is a long-term phenomenon, i.e., it needs time to become manifest. In the present analysis we demonstrate these facts, qualitatively and quantitatively, with a simple model which admittedly is only a caricature of cubic dice, yet we believe it shows the essential features of dice throwing.

II. MODEL

A. Theoretical setup

The first simplification is a reduction from the cube's six degrees of freedom (three each for translation and rotation) to three: we think of throwing the cube with one of its axes parallel to the floor, in such a way that it can only bounce on four edges and eventually comes to rest on one of only four faces. This would be equivalent to considering a square in a plane [5]. If we assign the same numbers to opposite sides of the square, the motion can effectively be modeled by a bar in the plane which has one rotational and two translational degrees of freedom, bouncing off the floor with either of its two ends. In the final state, the bar lies flat on the floor, with one or the other of the two tips lying to the right. The bar might be a homogeneous rod [4], but we choose to model it as a barbell, i.e., a massless rod with two point masses at its tips.

A general initial condition involves the position and velocity of the barbell's center of mass as well as its angle with respect to a fixed (horizontal) line and the corresponding angular velocity. Assuming that there is no horizontal force (gravity pulling downward and no horizontal momentum transfer during a bounce off the floor), the horizontal motion is uniform and may be ignored as irrelevant. This leaves us with only a vertical coordinate and the angle, plus the two corresponding velocities. As the center of mass reaches a maximum height between any two bounces, a complete set of trajectories can be characterized by three initial conditions: altitude of center of mass at zero vertical velocity, angle velocity, and angular velocity, see also Fig. 1. In the following analysis we fix the initial altitude and consider arbitrary combinations of initial angles and angular velocities in order to allow for two-dimensional renderings. The complete picture would involve a variation of the initial height as well.

The motion consists of two parts. The first is the combination of a free fall of the center of mass, and uniform rota-

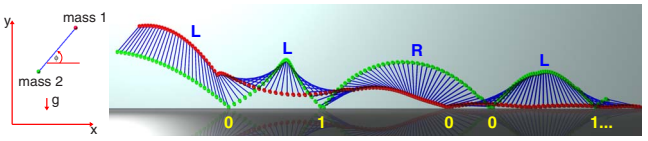

FIG. 1. (Color online) Schematic view of the model (left) and example of a trajectory and its symbolic characterization (right). A bounce is labeled by 0 when mass 1 is to the left of mass 2. The symbol for a bounce is 1 when mass 1 is to the right of mass 2. Note that this code does *not* reveal which ball is bouncing. When during a flight the barbell passes the vertical orientation clockwise we denote the passage by the letter *R*. A counterclockwise passage is denoted by *L*. No further symbol is added to the symbol sequence when the barbell has too little energy for vertical passages, that is, when the motion is restricted to either infinitely many type-0 or type-1 bounces. In addition, we omit repeating symbols at the end of the code and do not consider the (singular) case of a vertically hopping barbell with vanishing angular momentum. The symbol code for the example is *L*0*L*1*R*00*L*1.

tion of the barbell. The second part is the reflection off the ground when one of the two masses hits it. While the first part is classroom simple, the reflection law needs some attention, especially if we are to include dissipation in that process (see the Appendix for details of the bouncing with dissipation). Suffice it here to say that we introduce a friction parameter f to describe the reduction in vertical velocity of the bouncing mass, compared to what it would be in an elastic reflection. After the bounce, a new phase of free falling begins, with a positive upward velocity of the mass that hit the floor. This phase in turn ends when one of the masses touches the ground, and so on until the bar comes to rest lying flat.

B. Complexity

Even though these two alternating parts are extremely simple, their repetition may imply chaos (the situation is reminiscent of the "Galilean chaos" discussed in Ref. [9]). Let us now analyze its extent and nature, see Fig. 2. To this end we scan the plane of initial conditions at given height ($h=0.6$ in dimensionless units), angles (horizontal axis) ranging from 0 to 360 degrees, and angular velocities (vertical axis) from −7 to +7. Each point is given a color according to which final state is reached by the trajectory starting with these initial conditions: yellow if the final state is 0, cyan if it is 1 (see Fig. 1). In addition, the color code (inserted in the upper right of each picture) also reflects the number of bounces a trajectory performs before its energy is no longer sufficient for a turnover to the other configuration. This number depends strongly on the friction parameter. With low dissipation (upper left picture) a large number of bounces may be necessary before the final fate is determined. At high dissipation (lower right picture) the final state is reached much earlier.

The individual pictures, except Fig. 2(a), contain white lines which separate regions of different orbit classes as defined in Fig. 1, up to symbol lengths 4. Some of the classes are indicated by red symbols. In Fig. 2(a) we exhibit the points P_1 and P_2 which correspond to initial conditions where the barbell starts upright with zero angular velocity. The trajectories starting from there are not attracted by any of the two final states; instead, while losing energy in every bounce, they approach the unstable equilibria where the barbell stand upright on the floor, "not knowing" which way to fall. Of course this situation is unstable against small changes in the initial conditions, but the picture shows how these points are the organizing centers of the system's basins of attraction. The white lines emanating from P_1 and P_2 belong to the *stable manifolds* of the upright configuration, i.e., they represent trajectories which end up in the unstable equilibria. Clearly these lines mark the boundaries between the basins of attraction of the two final states, the stable equilibria. The white lines in Figs. 2(b)–2(d) are extensions of these lines. The red lines in Fig. 2(a), on the other hand, belong to the *unstable manifolds* of the upright configurations, i.e., they represent trajectories which would approach an upright configuration in backward time. The intersection points P_3 and P_4 of these lines are *heteroclinic points*; corresponding orbits originate from one upright configuration (at high initial energy) and up in the other (at rest). The figure shows that for small dissipation, the yellow parallelogram formed by points P_1 through P_4 (together with its cyan partner where the barbell is turned over) roughly delineates the border between predictability (inside) and nonpredictability (outside). With higher dissipation, the regions of regular behavior, hence of predictability, extend into regions of higher energy. Notice that increasing angular velocity at fixed initial altitude means higher total energy.

The pictures tell us that in order to observe randomness in the barbell's final states, we must start with sufficient initial energy, and preferably close to an upright configuration, so that several bounces with appreciable changes in orientation can take place before the final state is determined. This randomness, however, is not complete in the sense that we might zoom into the picture and find the basin boundaries entangled on all scales. Instead, the dissipation rather limits the development of chaos, or fractal geometry in phase space. This means that if a skilled player's hand can reproduce initial conditions with a small but finite margin, there is a good chance the desired final state will be attained. For more details on these matters, and an alternative representation of the system's phase space in terms of Poincaré surfaces of section, we refer to the Appendix.

III. CONCLUSIONS

In order to investigate the nature of pseudorandom chaotic behavior in the throwing of a dice we considered a minimal model which has only two final states rather than six. The system is sufficiently simple to allow for a detailed analysis of phase space structure with respect to position and extent of different types of motion, for which we introduced a symbolic orbit classification. The division of phase space into the basins of attraction of the two final states was represented in terms of sections (initial conditions at fixed height) where the geometry of the basin boundaries can be conveniently visualized. A particular organizing role for an understanding of

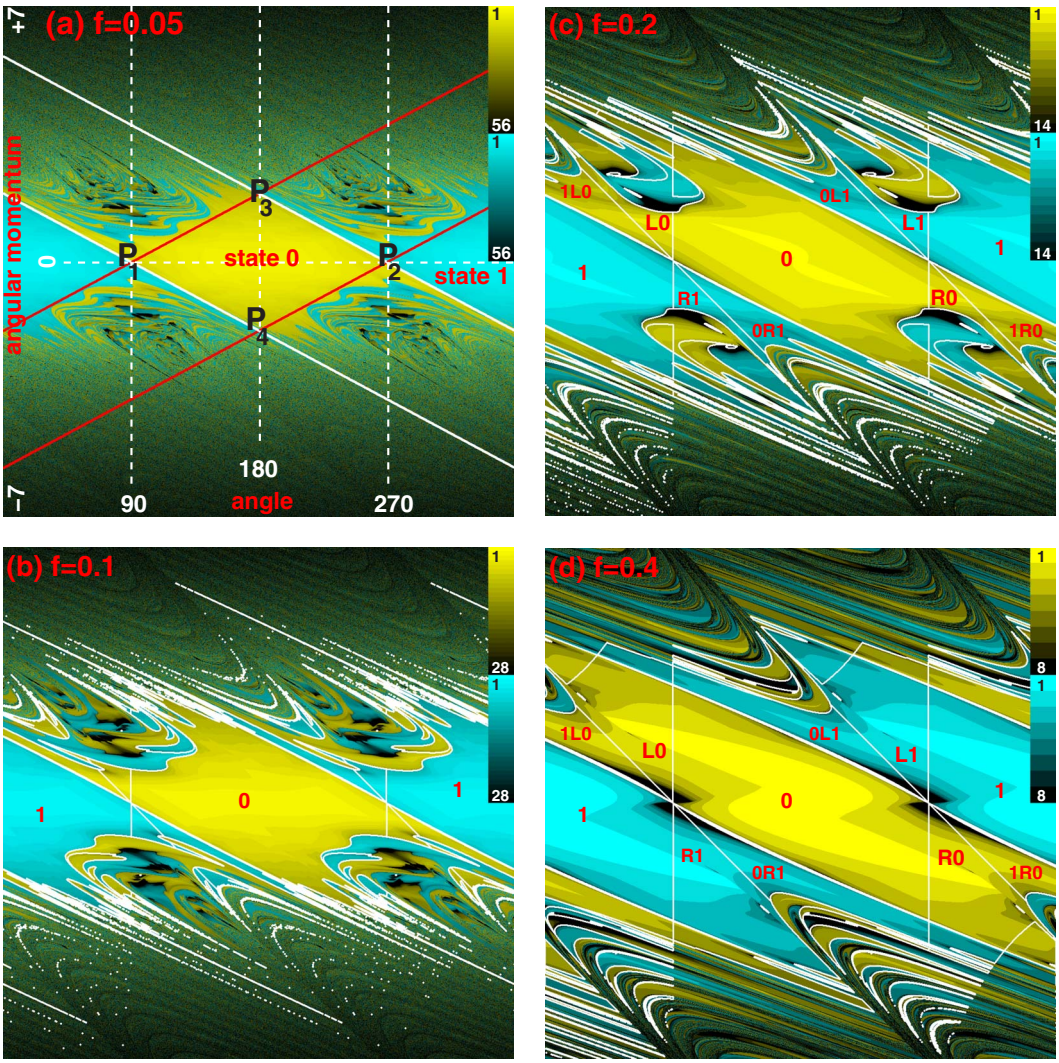

FIG. 2. (Color online) Final state diagrams for four friction values: (a) $f=0.05$, (b) $f=0.1$, (c) $f=0.2$, (d) $f=0.4$. Each diagram displays, in the plane of initial angles and angular velocities, the final outcome of the throw when the barbell has been dropped from an altitude $h_0=0.6$ above ground. Yellow (gray) points indicate final state 0: mass 1 is to the left of mass 2, cyan color (gray) marks points with final state 1: mass 1 is to the right of mass 2. The brightness of the color (grayscale) codes for the number of bounces before the barbell can no longer change its orientation; the darker the color (grayscale) the more bounces the system needs to fall below the critical energy value $E_c=0.5$. Black regions represent initial conditions where the barbell ends up standing almost upright on the ground, close to an unstable equilibrium state. (a) Friction strength $f=0.05$ with scales and axes (which are same in all other diagrams). The diagonal lines indicate the stable (white) and unstable (red and/or gray) directions of the linearized Poincaré map at the hyperbolic points P_1 and P_2; they are tangent in these points to their stable and unstable manifolds. Their intersections at points $P_{3,4}$, together with $P_{1,2}$, define a parallelogram which approximately delineates the separation of order from chaos. (b) Friction strength $f=0.1$; the white lines are boundaries of orbit type classes with symbol length up to 3. (c) $f=0.2$; symbol sequences of the simplest orbit type classes are displayed. (d) $f=0.4$, which corresponds to a realistic friction strength.

the system's complexity could be attributed to the stable and unstable invariant manifolds of the unstable equilibria, and their intersections. Using these features, we were able to roughly delineate a border between orderly regions of predictable behavior and chaos where the dependence on initial conditions is sensitive. This is particularly true in the limit of low dissipation, or almost Hamiltonian dynamics. For realistic friction strengths $f\approx 0.5$ [4] the typical number of bounces before the barbell can no longer change its orientation is about five bounces, as may be seen in Fig. 2(d). Hence, if a dice throw may be taken as a random number generator this is primarily because of the gambler's inability to reproduce initial conditions sufficiently well to ensure similar trajectories—and not so much because of an inherently strongly chaotic dynamics.

APPENDIX

Here we provide detailed information about our model and the numerical findings.

1. Model

We consider a barbell in the two-dimensional (x,y) plane, see Fig. 1. Two point masses are connected through a mass-

less rod of unit length $l=1$. In the derivation here, we consider the general case where the two masses m_1 and m_2 are not necessarily equal. Let us denote their positions by (x_1,y_1) and (x_2,y_2), respectively. We assume gravity to pull in the negative y direction, the floor being at $y=0$.

The barbell has three degrees of freedom, two for translation and one for rotation. A convenient representation is given by the center-of-mass coordinates (x,y) and the angle φ (see Fig. 1). Their connection to the coordinates of the mass points is

$$x_1 = x + \beta_2 \cos\varphi, \tag{A1}$$

$$x_2 = x - \beta_1 \cos\varphi, \tag{A2}$$

$$y_1 = y + \beta_2 \sin\varphi, \tag{A3}$$

$$y_2 = y - \beta_1 \sin\varphi. \tag{A4}$$

The $\beta_{1,2}$ are the mass ratios $\beta_1=m_1/(m_1+m_2)$ and $\beta_2=m_2/(m_1+m_2)$. Since $\beta_1+\beta_2=1$ we have only a single mass parameter. By choosing appropriate dimensionless units, all other parameters may be scaled away. The Lagrangian then reads

$$L = \frac{1}{2}(\dot{x}^2+\dot{y}^2) + \frac{1}{2}\beta_1\beta_2\dot{\varphi}^2 - y. \tag{A5}$$

In addition we might consider a reflecting potential at the floor, but the reflections at $y_1=0$ and $y_2=0$ will be given special attention in the following derivation of the bounce map. Note that above ground no force acts in the x direction, and we assume that also upon reflection there is no momentum change in x direction; hence $\dot{x}$ is a constant which we take to be 0, together with x. The system has effectively only two degrees of freedom, y and φ.

As long as the barbell falls freely, energy

$$E = \frac{1}{2}\dot{y}^2 + \frac{1}{2}\beta_1\beta_2\dot{\varphi}^2 + y \tag{A6}$$

and angular momentum $L=\beta_1\beta_2\dot{\varphi}$ are conserved. But what happens during reflection?

2. Bounce map with dissipation

Consider the case that the first particle hits the floor, $y_1=0$ or $y=-\beta_2\sin\phi$, at an angle $\pi<\varphi<2\pi$. It is then convenient to use the coordinates $y_1,\dot{y}_1$ instead of $y,\dot{y}$, and to express the energy (A6) as

$$E = \frac{1}{2}\frac{\beta_1}{\beta_1+\beta_2\cos^2\varphi}\dot{y}_1^2 + \frac{1}{2}\beta_2(\beta_1+\beta_2\cos^2\varphi)\left(\dot{\varphi} - \frac{\cos\varphi}{\beta_1+\beta_2\cos^2\varphi}\dot{y}_1\right)^2 - \beta_2\sin\varphi. \tag{A7}$$

The expression

$$\dot{\tilde{\varphi}} := \dot{\varphi} - \frac{\cos\varphi}{\beta_1+\beta_2\cos^2\varphi}\dot{y}_1 \tag{A8}$$

can be shown to be proportional, at given φ, to the tangential component of the momentum which does not change during the collision. Therefore we have the reflection conditions

$$(\varphi,\dot{\tilde{\varphi}}) \mapsto (\varphi',\dot{\tilde{\varphi}}) = (\varphi,\dot{\tilde{\varphi}}). \tag{A9}$$

As to $\dot{y}_1$, consider first the elastic collision where E is constant. Then Eq. (A7) tells us that at given $(\varphi,\dot{\tilde{\varphi}})$ and E there are two possible values of $\dot{y}_1$ which differ only in sign; the negative value corresponds to the incoming trajectory, the positive to the outgoing, and the reflection condition is $\dot{y}_1\mapsto\dot{y}_1'=-\dot{y}_1$. In the general case we assume the simplest version of an inelastic bounce,

$$\dot{y}_1 \mapsto \dot{y}_1' = -(1-f)\dot{y}_1, \tag{A10}$$

where $0\leqslant f\leqslant 1$ is the so-called coefficient of restitution. A vanishing value of f represents elastic reflection, and $f=1$ corresponds to the case where all vertical momentum is dissipated.

Equations (A9) and (A10) together give the reflection law

$$\begin{pmatrix}\varphi\\ \dot{\tilde{\varphi}}\\ \dot{y}_1\end{pmatrix} \mapsto \begin{pmatrix}\varphi'\\ \dot{\tilde{\varphi}}\\ \dot{y}_1'\end{pmatrix} = \begin{pmatrix}\varphi\\ \dot{\tilde{\varphi}}\\ -(1-f)\dot{y}_1\end{pmatrix}$$

$$(y_1 = y_1' = 0,\ \pi<\varphi<2\pi), \tag{A11}$$

the change in energy being

$$\Delta = E - E' = \frac{f(2-f)}{2}\frac{\beta_1\dot{y}_1^2}{\beta_1+\beta_2\cos^2\varphi}. \tag{A12}$$

The energy loss is strongest, $\Delta=\frac{1}{2}f(2-f)\dot{y}_1^2$, when the bounce is head on, $\varphi=3\pi/2$.

In case mass 2 bounces off the floor, $y_2=0$ and $0<\varphi<\pi$, the formulas (A7)–(A12) remain the same except for the replacements $y_1\to y_2$, $\beta_{1,2}\to\beta_{2,1}$, $\sin\varphi\to-\sin\varphi$, and $\cos\varphi\to-\cos\varphi$.

The complete motion of the barbell is described by

$$\ddot{y} = -1 \quad \text{and} \quad \ddot{\varphi} = 0 \tag{A13}$$

as long as both $y_1>0$ and $y_2>0$, and by the above reflection laws if either $y_1=0$ or $y_2=0$.

3. Phase space structure: Poincaré section

Recall that the system has two parameters, the mass ratio $\beta_1=1-\beta_2$ and the friction coefficient f, and that its phase space has four dimensions, with configuration space $\mathrm{S}(\varphi)\times\mathbb{R}(y)$ and momenta $(p_\varphi,p_y)=(\beta_1\beta_2\dot{\varphi},\dot{y})\in\mathbb{R}^2$. Except for $f=0$ (where $E=$const) there exists no constant of motion. The points of minimum energy $E=0$, $(\varphi,\dot{\varphi},y,\dot{y})=(0,0,0,0)$ and $(\pi,0,0,0)$, are the two possible final states 1 and 0, respectively. Together they attract the entire phase space, except for the boundary between their basins of attraction. This boundary is formed by the three-dimensional (3D)

stable manifolds of the two unstable fixed points $(\varphi,\dot{\varphi},y,\dot{y})=(\pi/2,0,\beta_1,0)$ with energy $E=\beta_1$, and $(\varphi,\dot{\varphi},y,\dot{y})=(3\pi/2,0,\beta_2,0)$ with energy $E=\beta_2$. These points correspond to the barbell standing upright with either mass 2 or mass 1 touching the ground, "not knowing" which way to fall over. Their stable manifolds consist of the $(y,\dot{y})$ planes defined by $(\varphi,\dot{\varphi})=(\pi/2,0)$, with $E>\beta_1$, and $(\varphi,\dot{\varphi})=(3\pi/2,0)$ with $E\geqslant\beta_2$, plus the sets of initial conditions which are drawn towards these planes. The aim of our analysis is to understand how these manifolds partition the phase space into the two basins of attraction.

A convenient way of studying this phase space structure is in terms of suitably chosen Poincaré sections, thereby reducing the system's dimension by one. A section condition is "suitable" if

(a) every orbit intersects it sufficiently many times to reveal its nature and its final state,

(b) the surface of section can be represented in a one-to-one projection.

An obvious choice of this kind is to consider the barbell's motion at the moments immediately after it bounces off the floor, i.e., at $y_1=0$ with $\dot{y}_1>0$ $(\pi<\varphi<2\pi)$ and $y_2=0$ with $\dot{y}_2>0$ $(0<\varphi<\pi)$. This condition is met infinitely many times by every orbit, hence it is *complete* in the sense defined in [13]. It produces a 3D surface of section through the 4D phase space. But which coordinates do we choose to represent this surface? We might think of $(\varphi,\dot{\varphi},E)$, but note from Eq. (A7) that a given set $(\varphi,\dot{\varphi},E)$ together with $y_1=0$ $(\pi<\varphi<2\pi)$ would not in general allow us to determine a unique $\dot{y}_1>0$ (there may be two such values, or none). However, if we use the coordinates $(\varphi,\tilde{\dot{\varphi}},E)$, then Eq. (A7) becomes

$$E=\frac{1}{2}\frac{\beta_1}{\beta_1+\beta_2\cos^2\varphi}\dot{y}_1^2+\frac{1}{2}\beta_2(\beta_1+\beta_2\cos^2\varphi)\tilde{\dot{\varphi}}^2-\beta_2\sin\varphi, \tag{A14}$$

which shows that $\dot{y}_1>0$ is indeed uniquely determined by $(\varphi,\tilde{\dot{\varphi}},E)$. The corresponding initial conditions $(\varphi,\dot{\varphi},y,\dot{y})$ right after the bounce are then given with

$$\dot{\varphi}=\tilde{\dot{\varphi}}+\frac{\cos\varphi}{\beta_1+\beta_2\cos^2\varphi}\dot{y}_1,\quad y=-\beta_2\sin\varphi,$$

$$\dot{y}=\dot{y}_1-\beta_2\dot{\varphi}\cos\varphi, \tag{A15}$$

and similarly for bounces of mass 2 if $0<\varphi<\pi$.

The 3D surface of section $\mathcal{P}$ is that part of $\mathrm{S}(\varphi)\times\mathbb{R}(\tilde{\dot{\varphi}})\times\mathbb{R}(E)$ where $E\geqslant 0$ and $\dot{y}_{1,2}^2\geqslant 0$; using Eq. (A14) and the corresponding equation for reflection of mass 2, we find that the allowed values of $\tilde{\dot{\varphi}}$, at given E (see Fig. 3), are restricted by

$$0\leqslant\tilde{\dot{\varphi}}^2\leqslant\frac{2}{\beta_2}\frac{E+\beta_2\sin\varphi}{\beta_1+\beta_2\cos^2\varphi}\quad(\pi<\varphi<2\pi),$$

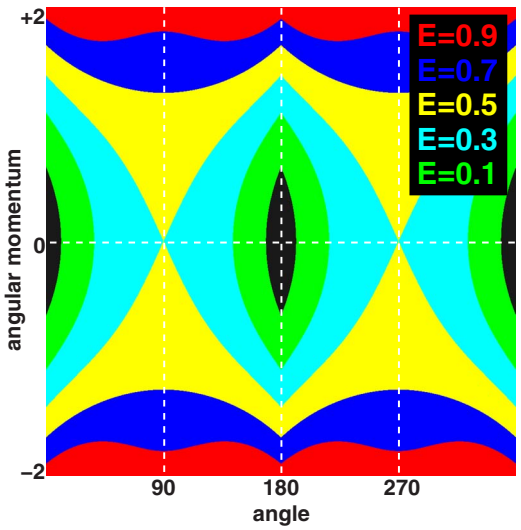

FIG. 3. (Color online) Accessible regions for the surface of section given by Eq. (A16) for five energy levels. The region in black is accessible for all examples. For $E=0.3$ green (gray) regions become accessible, too, for $E=0.5$ the regions in cyan (gray), for $E=0.7$ the yellow regions (gray), and finally, for $E=0.9$ also the blue (gray) regions. The region in red (gray) is inaccessible for all these energy levels.

$$0\leqslant\tilde{\dot{\varphi}}^2\leqslant\frac{2}{\beta_2}\frac{E-\beta_1\sin\varphi}{\beta_1+\beta_2\cos^2\varphi}\quad(0<\varphi<\pi). \tag{A16}$$

The Poincaré map $P:\mathcal{P}\to\mathcal{P}$ is the mapping

$$\begin{pmatrix}\varphi\\ \tilde{\dot{\varphi}}\\ E\end{pmatrix}\mapsto\begin{pmatrix}\varphi'\\ \tilde{\dot{\varphi}}\\ E'\end{pmatrix}=P\begin{pmatrix}\varphi\\ \tilde{\dot{\varphi}}\\ E\end{pmatrix}=R\circ F\begin{pmatrix}\varphi\\ \tilde{\dot{\varphi}}\\ E\end{pmatrix}=R\begin{pmatrix}\varphi'\\ \tilde{\dot{\varphi}}\\ E\end{pmatrix}, \tag{A17}$$

where F describes the flight (A13) to the next bounce, and R the reflection (A11) (or the corresponding law if $y_2=0$). Notice from the previous section that the new coordinates $(\varphi',\tilde{\dot{\varphi}}')$ are determined by the flight F alone, while the energy changes only in the reflection, according to Eq. (A12).

The stable equilibria $(\varphi,\tilde{\dot{\varphi}},E)=(0,0,0)=:S_1$ and $(\pi,0,0)=:S_2$ belong to $\mathcal{P}$, as do the unstable equilibria $(\varphi,\tilde{\dot{\varphi}},E)=(\pi/2,0,\beta_1)=:U_1$ and $(3\pi/2,0,\beta_2)=:U_2$. The stable manifolds $\mathcal{W}_{1,2}\subset\mathcal{P}$ of $U_{1,2}$ are 2D surfaces which contain the lines $(\pi/2,0,E\geqslant\beta_1)$ and $(3\pi/2,0,E\geqslant\beta_2)$, plus all points which are attracted to these lines under P.

Let us think of $\mathcal{P}$ as being made up of $(\varphi,\tilde{\dot{\varphi}})$ slices at constant E. In case the collision is elastic, these slices are invariant planes, and we may study the Poincaré map at fixed energy. Since P is not smooth at $\varphi=0$ or π, the points $(0,0,E)$ and $(\pi,0,E)$ do not exhibit the typical elliptic character of stable points in analytic maps. However, the unstable points $(\pi/2,0,E)=:P_1$ $(E>\beta_1)$ and $(3\pi/2,0,E)=:P_2$ $(E>\beta_2)$ are typical hyperbolic points, and we may consider the linearized map in their neighborhoods. To do so we start with an initial condition

$$(\varphi(0),\dot{\tilde{\varphi}}(0),E)=(3\pi/2+\alpha,\omega,E), \tag{A18}$$

assuming α and ω to be infinitesimally small, and determine α', ω' in

$$(\varphi(t),\dot{\tilde{\varphi}}(t),E)=(3\pi/2+\alpha',\omega',E), \tag{A19}$$

to linear order in α, ω, where t is the time of the next bounce. Using Eq. (A14) we obtain $\dot{y}_1(0)=\sqrt{2(E-\beta_2)}+O(2)$, where $O(2)$ means second order in (α,ω), and with Eq. (A15) we obtain the initial values

$$\dot{\varphi}(0)=\omega+\frac{\alpha}{\beta_1}\sqrt{2(E-\beta_2)}+O(2),$$

$$y(0)=\beta_2+O(2),$$

$$\dot{y}(0)=\sqrt{2(E-\beta_2)}+O(2). \tag{A20}$$

The flight between the bounces is then given by $y(t)=y(0)+\dot{y}(0)t-\frac{1}{2}t^2$ and $\varphi(t)=\varphi(0)+\dot{\varphi}(0)t$. The time t of the next bounce is determined from $y(t)=-\beta_2 \sin\varphi(t)$ which we solve by expanding the right-hand side to second order in t: $t=2\dot{y}(0)+O(2)$. This implies (omitting the higher orders)

$$\varphi(t)=\varphi(0)+2\dot{y}(0)\dot{\varphi}(0), \quad \Rightarrow \alpha'=\alpha+2\dot{y}(0)\dot{\varphi}(0),$$

$$\dot{y}(t)=-\dot{y}(0)=-\sqrt{2(E-\beta_2)}=\dot{y}_1(t),$$

$$\dot{\tilde{\varphi}}(t)=\dot{\varphi}(0)-\frac{\alpha'}{\beta_1}\dot{y}_1(t), \quad \Rightarrow \omega'=\dot{\varphi}(0)+\frac{\alpha'}{\beta_1}\dot{y}(0). \tag{A21}$$

Inserting $\dot{\varphi}(0)=\omega+\dot{y}(0)\alpha/\beta_1$ on the right-hand side of the equations for α' and ω', we finally obtain the mapping

$$\begin{pmatrix}\alpha'\\ \omega'\end{pmatrix}=\begin{pmatrix}1+(4/\beta_1)(E-\beta_2) & 2\sqrt{2(E-\beta_2)}\\ (2/\beta_1)\sqrt{2(E-\beta_2)}[1+(2/\beta_1)(E-\beta_2)] & 1+(4/\beta_1)(E-\beta_2)\end{pmatrix}\begin{pmatrix}\alpha\\ \omega\end{pmatrix}. \tag{A22}$$

Since both α' and ω' do not change upon reflection, this already describes the full Poincaré map (as $E'=E$). Nothing in these arguments needs to be modified if dissipation is taken into account. The only change happens when energy is lost in the reflection process; using Eq. (A12) we see that Eq. (A22) needs to be complemented by

$$E'=\beta_2+(1-f)^2(E-\beta_2), \tag{A23}$$

which means the Poincaré map takes us from the energy slice E to the energy slice E', which approaches β_2 in a geometric manner.

The eigenvalues $\lambda_{s,u}$ (stable and unstable, respectively) and eigenvectors of the mapping (A22) are

$$\lambda_{s,u}=1+\frac{4}{\beta_1}(E-\beta_2)\mp\frac{2}{\beta_1}\sqrt{2(E-\beta_2)[\beta_1+2(E-\beta_2)]}, \tag{A24}$$

$$\begin{pmatrix}\alpha\\ \omega\end{pmatrix}\propto\begin{pmatrix}\beta_1\\ \mp\sqrt{\beta_1+2(E-\beta_2)}\end{pmatrix}, \tag{A25}$$

the upper (lower) sign referring to the stable (unstable) direction. They do not depend on the friction parameter f but on the energy. As $E\to\beta_2$ they are (up to a factor) $(\alpha,\omega)=(\beta_1,\mp 1/\sqrt{\beta_1})$, and as $E\to\infty$ we have $(\alpha,\omega)\to(\beta_1,\mp\sqrt{2E})$.

According to the stable and unstable manifold theorem the manifolds $\mathcal{W}^{s,u}_{1,2}$ are tangent to these eigenvectors. The unstable manifolds $\mathcal{W}^{u}_{1,2}$ can be obtained by forward iteration of little segments on the unstable eigendirections, the stable manifolds $\mathcal{W}^{s}_{1,2}$ by backward iteration of little segments on the stable eigendirections. The manifolds $\mathcal{W}^{u}_{1,2}$ extend down to the stable fixed points at energy $E=0$ whereas the stable manifolds $\mathcal{W}^{s}_{1,2}$ exist only at energies $E>\beta_{1,2}$, respectively. The stable manifolds represent the boundaries between the basins of attraction of the final states 1 and 0.

4. Final state diagrams

Given the complexity of the motion, it appears impossible to give a rendering of the three-dimensional surface of section $\mathcal{P}$ and its division by the two-dimensional manifolds $\mathcal{W}^{s,u}_{1,2}$. Therefore we propose to consider *final state diagrams*, i.e., $(\varphi,\dot{\tilde{\varphi}})$ sections at constant energy E where each point is given a color according to whether it is attracted to the final state 1 (cyan) or 0 (yellow), see Fig. 4 for $E=1.0$ and five different values of f. Obviously, if $E<\min(\beta_1,\beta_2)$, then the upright positions $\dot{\varphi}=\pi/2$ or $3\pi/2$ cannot be reached, hence the final state is uniquely determined. In the following we assume $\beta_1=\beta_2=1/2$, so when $E<1/2$ the final state is 1 if $-\pi/2<\varphi<\pi/2$ and 0 if $\pi/2<\varphi<3\pi/2$. In the final state diagrams of Fig. 4 the colors also reveal the number of bounces necessary to reach $E<1/2$: they become darker as this number increases. We also show the stable and unstable eigendirections of the hyperbolic points P_1 and P_2. The stable directions agree with the separation of colors, i.e., with the boundaries of the two basins of attraction, even a considerable distance away from $P_{1,2}$. At high values of f as, e.g., at $f=0.4$, the basin boundaries exhibit a rather smooth and clear-cut character. However, as f decreases they become more and more fractal-like.

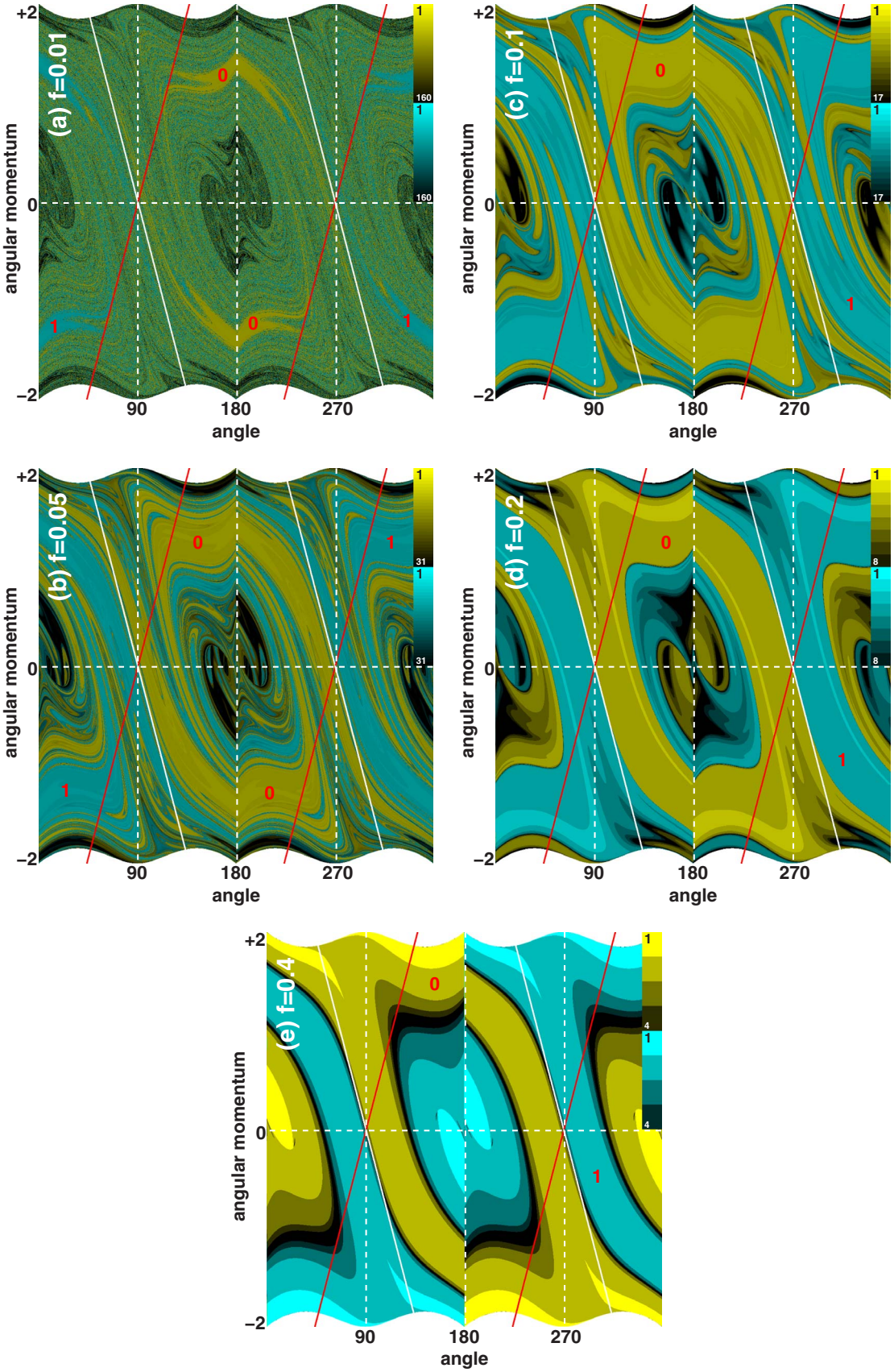

FIG. 4. (Color online) Final state diagrams for a $(\varphi, \tilde{\varphi})$ slice at $E_0=1.0$. Friction values: (a) $f=0.01$, (b) $f=0.05$, (c) $f=0.1$, (d) $f=0.2$, and (e) $f=0.4$. A point is given the color cyan and/or gray (yellow and/or gray) if upon iteration of the Poincaré map it ends up in the state 0 (or 1); the darkness reflects the number of iterations necessary for E to become less than $1/2$ (see insets at the upper right for scales).

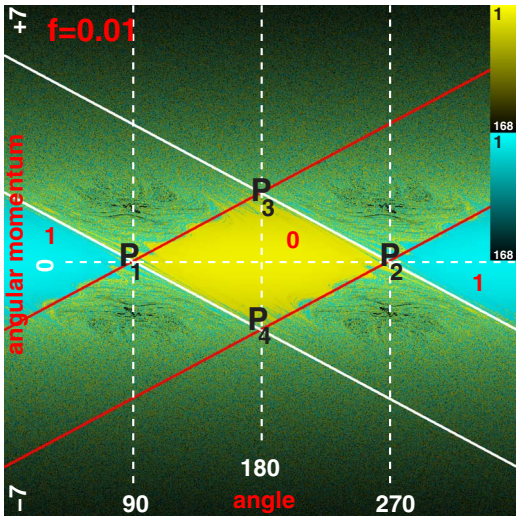

FIG. 5. (Color online) Final state diagram at $h=0.6$ for the low friction parameter $f=0.01$. All scales and ranges are the same as in Fig. 2.

Physical intuition suggests to define yet another kind of final state diagram. It is derived from the Poincaré section condition $\dot{y}=0$ and $\ddot{y}<0$, i.e., we consider those points of a trajectory where the center of mass reaches a local maximum. The 3D section of phase space so defined may be parametrized by the coordinates $(\varphi,\dot{\varphi},y)$, and from Eq. (A6) we see that the 2D subsets $E=$const are parabolas in the $(\dot{\varphi},y)$ plane, independent of φ except for the fact that the bouncing conditions $y_1>0$ and $y_2>0$ require $y>-\beta_2 \sin\varphi$ $(\pi<\varphi<2\pi)$ and $y>\beta_1 \sin\varphi$ $(0<\varphi<\pi)$. A given point $(\varphi,\dot{\varphi},y)$ (together with $\dot{y}=0$ immediately defines an initial condition, and the Poincaré map is defined by three steps: (i) downward flight $\varphi(t)=\varphi(0)+\dot{\varphi}(0)t$ and $y(t)=y(0)-\frac{1}{2}t^2$, (ii) reflection at the bottom $y_1=0$ or $y_2=0$, (iii) upward flight until the condition $\dot{y}(t)=0$ is met again. If we took coordinates $(\varphi,\dot{\varphi},E)$, a similar analysis as the above might be performed in terms of $(\varphi,\dot{\varphi})$ slices at constant energy, with a decrease of E according to Eq. (A12) according to where the bounce took place. However, the physically more directly appealing coordinates $(\varphi,\dot{\varphi},y)$ suggest to look at $(\varphi,\dot{\varphi})$ slices with fixed $y=h$. This would not be suitable for the definition of a meaningful Poincaré map because the values y change at each iteration, even at zero dissipation $f=0$, and if $f>0$ there is a general tendency for the maximum height to decrease so that a given slice would only be met a finite number of times.

This argument does not prevent us from looking at final state diagrams in a $(\varphi,\dot{\varphi})$ slice with initial value $y=h$. Here we consider a set of initial conditions where the barbell starts at height h with no vertical velocity, but any combination of $(\varphi,\dot{\varphi})\in \mathrm{S}(\varphi)\times\mathbb{R}(\dot{\varphi})$; the energy $E\geqslant h$ as given by Eq. (A6) becomes arbitrarily large as $\dot{\varphi}^2$ increases. In order to see how the invariant manifolds of the lines above $(\varphi,\dot{\varphi},y)=(\pi/2,0,\beta_1)$ and $(3\pi/2,0,\beta_2)$ intersect these slices, we consider an initial condition $(\varphi,\dot{\varphi},y)=(3\pi/2+\bar{\alpha},\bar{\omega},h)$ with infinitesimal $(\bar{\alpha},\bar{\omega})$ and determine where the trajectory

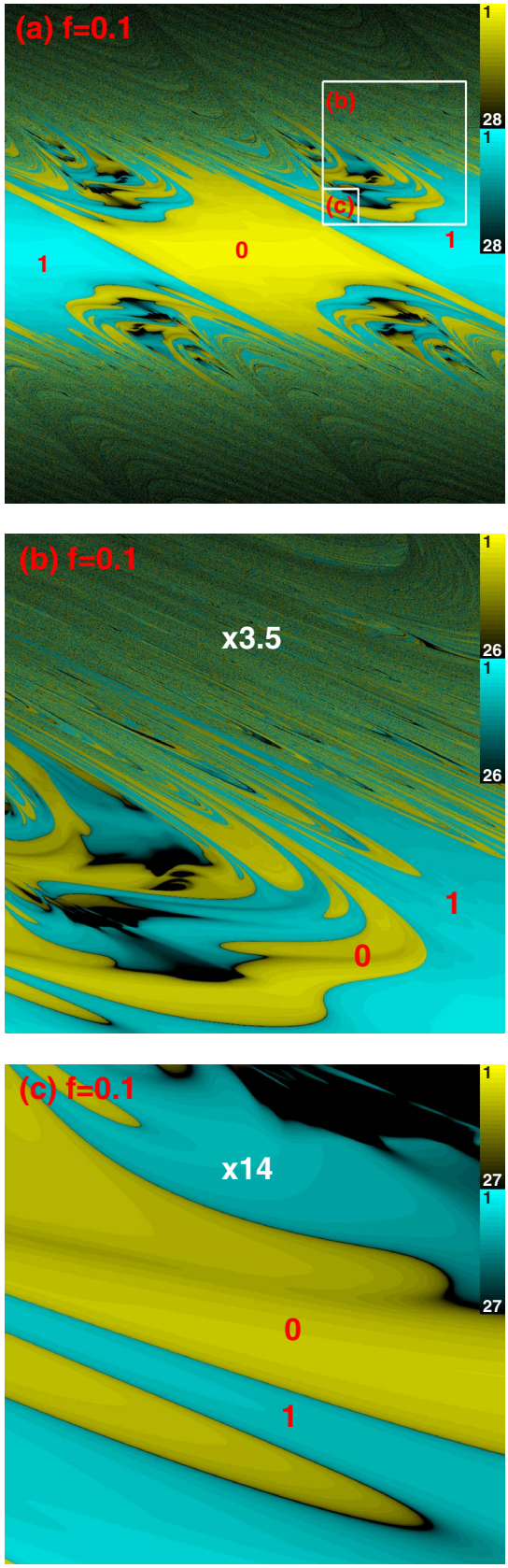

FIG. 6. (Color online) Final state diagram for $h=0.6$ and $f=0.1$ with two successive blowups. (a) Scales and ranges as in Fig. 2, (b) 3.5-fold magnification of the region marked in (a), (c) 14-fold magnification.

$$\bar{\alpha}(t) = \bar{\alpha} + \bar{\omega}t, \quad y(t) = h - \frac{1}{2}t^2 \tag{A26}$$

intersects the Poincaré surface $y_1=0$, $\dot{y}_1>0$. An elementary calculation, to linear order in $(\bar{\alpha},\bar{\omega})$ gives $t=\sqrt{2(h-\beta_2)}$ and, with $\dot{\tilde{\varphi}} := \omega$ as before,

$$\begin{pmatrix} \alpha(t) \\ \omega(t) \end{pmatrix} = \begin{pmatrix} 1 & \sqrt{2(h-\beta_2)} \\ (1/\beta_1)\sqrt{2(h-\beta_2)} & 1+(2/\beta_1)(h-\beta_2) \end{pmatrix} \begin{pmatrix} \bar{\alpha} \\ \bar{\omega} \end{pmatrix}. \tag{A27}$$

From Eq. (A25) we know the tangent vectors to the invariant manifolds in the Poincaré surface $y_1=0$, $\dot{y}_1>0$. Therefore, inverting Eq. (A27) with $(\alpha(t),\omega(t))$ along the eigendirections, we obtain the tangent vectors to the invariant manifolds in the $(\bar{\alpha},\bar{\omega})$ plane:

$$\begin{pmatrix} \bar{\alpha} \\ \bar{\omega} \end{pmatrix} \propto \begin{pmatrix} \sqrt{\beta_1+2(h-\beta_2)} \\ \mp 1 \end{pmatrix}. \tag{A28}$$

Again the upper sign refers to the stable, the lower to the unstable direction. (If the bounce occurs at $y_2=0$, β_1 and β_2 must be exchanged.) In the linear neighborhood of the points $(\varphi,\dot{\varphi})=(\pi/2,0)$ and $(3\pi/2,0)$, these directions depend on E but not on the friction parameter f; they are symmetric with respect to the φ axis. The linear approximation to the invariant manifolds seems to be good at least up to their first intersection in the points $P_{3,4}=\{\pi,\pi/[2\sqrt{\beta_1+2(h-\beta_2)}]\}$ as Fig. 2 and Fig. 5 illustrate.

One might be tempted to interpret $P_{3,4}$ in Fig. 5 as heteroclinic points, but that becomes meaningful only in the limit of vanishing f: their forward images tend to lie in slices with lower values of y whereas the backward images tend to have larger y. Nevertheless it is obvious that the diagrams reveal some degree of heteroclinic entanglement. Its depth in scale, however, is limited by friction. The two blowups in the final state diagram, Fig. 6, show that upon sufficient magnification the basin boundaries become smooth. The situation is similar to that of a steel pendulum over three magnets, if air drag is taken into account [10,11]; there the limits to fractality were analyzed in [12].

The final state diagrams of Figs. 2, 5, and 6 illustrate how regions of order (predictability) and chaos (strong dependence on initial conditions) depend on initial conditions and the parameter f (the parameter h might also be considered, but we took $h=0.6$ in all cases).

[1] See the Wikipedia article on dice at http://en.wikipedia.org/wiki/Dice

[2] M. Born, *Physics in My Generation* (Springer, New York, 1969), p. 113.

[3] P. Diaconis, S. Holmes, and R. Montgomery, SIAM Rev. **49**, 211 (2007); see also at http://www.geocities.com/dicephysics.

[4] V. Z. Vulović and R. E. Prange, Phys. Rev. A **33**, 576 (1986).

[5] R. Feldberg, M. Szymkat, C. Knudsen, and E. Mosekilde, Phys. Rev. A **42**, 4493 (1990).

[6] J. Ford, Phys. Today **36** (4), 40 (1983).

[7] Zhang Kechen, Phys. Rev. A **41**, 1893 (1990).

[8] D. B. Murray and S. W. Teare, Phys. Rev. E **48**, 2547 (1993).

[9] P. H. Richter, in *The Emergence of Complexity in Mathematics, Physics, Chemistry, and Biology*, Proceedings of the Plenary Sessions of the Pontifical Academy of Sciences, 1992, edited by B. Pullman (Pontifical Academy of Sciences, Vatican, 1994), pp. 103–127.

[10] T. Tél and M. Gruiz, *Chaotic Dynamics. An Introduction Based on Classical Mechanics* (Cambridge University Press, Cambridge, 2006).

[11] H.-O. Peitgen, H. Jürgens, and D. Saupe, *Chaos and Fractals: New Frontiers of Science*, 2nd ed. (Springer, Berlin, 2004).

[12] H. Pleteit, Diploma Thesis, Bremen University, Germany, 1995.

[13] H. R. Dullin and A. Wittek, J. Phys. A **28**, 7157 (1995).